

## Modeling triblock surfactant-templated mesostructured cellular foams

Supriyo Bhattacharya<sup>a)</sup> and Keith E. Gubbins

Center for High Performance Simulation and Department of Chemical and Biomolecular Engineering,  
North Carolina State University, Raleigh, North Carolina 27695-7905

(Received 13 June 2005; accepted 11 July 2005; published online 6 October 2005)

Lattice Monte Carlo simulations are used to understand the role of surfactant self-assembly in the synthesis of templated mesoporous materials with ultralarge pores. Our system consists of model triblock surfactants in the presence of oil, water, and inorganic oxide. Depending on the temperature and component concentrations, these systems phase separate, and the surfactant-rich phase forms structures such as cylinders, lamellae, and spheres ordered in repetitive arrangements. In the absence of oil, the structures are cylindrical with diameters of 100 Å, but increasing oil concentration produces ultralarge spheres with diameters above 500 Å. Our results closely resemble the cylinder to sphere transition associated with the synthesis of the mesostructured cellular foams (MCFs). Pore size distributions of our model structures are qualitatively comparable with the pore size distributions of MCFs obtained from adsorption experiments. We also observe an increase in average pore size with oil concentration, which is consistent with the experimental reportings.  
© 2005 American Institute of Physics. [DOI: 10.1063/1.2013250]

### I. INTRODUCTION

Templated mesoporous materials have been reported in literature for more than three decades and patents were filed in this area as early as 1969.<sup>1</sup> In the early 1990s, different research groups independently discovered two similar structured mesoporous silicas. One was folded silica material-16 (FSM-16),<sup>2</sup> synthesized by Yanagisawa *et al.*, and the other was mobile crystalline material-41 (MCM-41),<sup>3,4</sup> synthesized by Beck and co-workers. Today, variations in methodologies and ingredients are continuously leading to the discovery of new materials. Leaving aside subtle differences, the generalized synthesis starts with the preparation of a surfactant/oil/water solution at a controlled temperature. An inorganic oxide (usually silica) source is then added to this solution, producing a surfactant-silica liquid-crystal phase which serves as a template. Polymerization of silica takes place via the sol-gel process, producing a solid framework around the liquid crystals. The solution is then dried and the polymerized residues calcined to produce the final mesoporous material. The process is sensitive to the parameters such as the chain architecture and length, temperature and pH of the solution, and the different component concentrations.

Here, we present a molecular simulation strategy that mimics the synthesis of mesostructured cellular foam (MCF), whose pore structure consists of large spherical cells with diameters between 100 and 500 Å. The cells are connected to each other via windows having a relatively smaller diameter, around 100 Å (Fig. 1). MCFs have exceptionally large pores compared to most other mesoporous materials, whose pore diameters are usually below 200 Å. The well-defined ordered structures are obtained even at the highest pore sizes, whereas attempts to increase the pore size in MCM materials beyond a certain limit have resulted in

poorly ordered or disordered materials.<sup>5</sup> The large pore sizes of MCFs make them suitable candidates for separation applications involving macromolecules.

MCFs can be synthesized using pluronic triblock surfactants as templates, but they require the presence of a hydrophobic solvent in the surfactant solution. The detailed synthesis may be obtained from Lettow *et al.*<sup>6</sup> Usually, the surfactant used in the synthesis is pluronic P123, and the hydrophobic solvent is trimethyl benzene or TMB, which is frequently referred to as “oil” in literature. Pluronics have the general formula  $(\text{PEO})_x(\text{PPO})_y(\text{PEO})_x$ , where PEO denotes polyethylene and PPO denotes polypropylene. For P123,  $x$  is 20 and  $y$  is 70. In pluronic surfactants, PEO acts as the hydrophilic group and PPO acts as the hydrophobic group. In the absence of oil, the pore geometry obtained by polymerizing silica around P123 micelles is cylindrical in nature with pore diameters of around 100 Å. This cylindrical shape is maintained even when a small amount of oil is added during synthesis. The interesting transition occurs when the oil concentration is increased beyond a certain threshold. This causes the pores to become spherical, and the pore size increases rapidly as the oil concentration is increased. This transition from cylindrical SBA-15 to spherical MCF is the topic of discussion in several recent publications.<sup>6-9</sup> Change in pore geometry with concentration is a phenomenon known to be associated with the synthesis of mesoporous material.<sup>10</sup> For example, while synthesizing MCM materials, it is observed that increasing the surfactant concentration leads to the formation of lamellar instead of cylindrical pores. However, such transitions do not accompany any significant change in the pore size. On the other hand, the transition from SBA-15 to MCF brought about by TMB is accompanied by a threefold increase in the pore size, while maintaining a strong stability of the porous structure.

In order to understand the thermodynamic reasons that eventually lead to the ultralarge pores in MCF, we need to

<sup>a)</sup>Electronic mail: sbhatta@unity.ncsu.edu

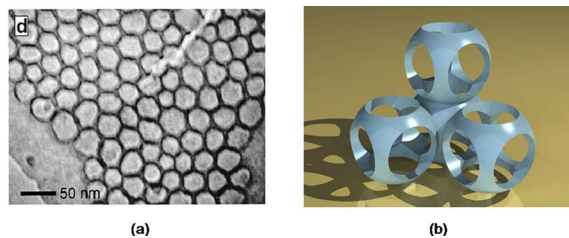


FIG. 1. (Color online) (a) TEM of MCF. Reprinted in part with permission from Schmidt-Winkel *et al.* © 2000 American Chemical Society, and (b) graphical schematic of MCF.

investigate the phenomena of surfactant self-assembly. The two major opposing forces which generate the ordered structures in a surfactant solution are (1) the hydrophobic effect, that tends to bring all the surfactant tails together, and (2) the ionic/steric repulsion of the head groups, that restricts the number of chains in a micelle to a maximum limit. In a real system, there can be numerous other factors which fine-tune the geometry of the final structure. These include the temperature, hydrogen bonding,  $pH$ , and the solvent interactions. Many of these effects are not clearly understood, and including all of these in a computer simulation poses a difficult task. In Sec. II, we discuss the methodology we have used for modeling the self-assembling surfactant system.

Atomistic simulations (Monte Carlo and molecular dynamics) cannot access the large system sizes (hundreds of nanometers) needed to represent MCF and its synthesis. In this work, we employ the lattice Monte Carlo simulation methods, which enable the use of mesoscopic models of polymeric chains. Lattice Monte Carlo models have been used extensively to study the properties of surfactant solutions<sup>11,12</sup> and mesoporous material synthesis.<sup>9,13,14</sup> Larson *et al.*<sup>15</sup> and Larson<sup>16</sup> were the first to use the lattice models for studying surfactant self-assembly. Siperstein and Gubbins developed the models for MCM materials that showed qualitative agreement with the experimental results for heat of adsorption. In this paper, we focus on the fundamental features of the surfactant system which we believe are responsible for the formation of the cellular cavities in MCFs; namely, the triblock architecture, relative strengths of the hydrophobic and hydrophilic potentials, and component concentrations. From our simulation results using elongated boxes, we are able to construct the ternary and quaternary phase diagrams of surfactant-oil-water-silica systems, and observe the formation of the different liquid-crystal phases.

## II. SIMULATION METHOD

In order to simulate the synthesis of mesoporous silicas, we modeled the surfactants and solvents as coarse-grained models, and sampled the system using lattice Monte Carlo simulations. The simulation box consists of a cubic lattice, where one lattice unit is equivalent to 36 Å. We obtained this lattice length as follows. The fully extended chain length of a P123 molecule was estimated by optimizing the molecular geometry using the mean-field approximation. The length was found to be 400 Å. This was equated to the length of a model surfactant chain, which is 11 lattice units. Therefore, one lattice unit can be calculated as  $400/11 \approx 36$  Å. Compar-

ing the surfactant chain lengths in the simulation and experimental systems is a logical way of mapping the two systems, because the diameter of a liquid crystal is mainly governed by the length of the surfactant. The solvents (water and oil) are modeled as spherical beads occupying one lattice unit each. The surfactant is modeled as a string of beads with each bead occupying one lattice unit along with an additional criterion that these beads will occupy adjacent lattice sites. In the model surfactant, several monomer units are represented by a single lattice bead. After carrying out simulations with different numbers of monomers per bead, we found that, 6.67 polyethylene units for a head bead and 14 polypropylene units for a tail bead are sufficient to give cylindrical structures in the absence of oil. This ensured that our model is realistic enough to follow the experimental trends. We therefore selected our model surfactant to be  $H_3T_5H_3$  ( $H$ : head and  $T$ : tail) by scaling down the surfactant P123 used in the synthesis of MCF. Interactions between the different components are modeled as the square-well potentials. Two beads,  $i$  and  $j$  interact with a potential  $\varepsilon_{ij}$ , if they are adjacent to one another, and zero if farther away. Using the fact that the number of molecules in a  $NVT$  ensemble does not change over the course of a simulation, it can be proved that the energy change associated with any configuration rearrangement depends only on the exchange energies. An exchange energy,  $w_{ij}$  can be derived from the individual interaction potentials using the equation,

$$w_{ij} = \varepsilon_{ij} - \frac{1}{2}(\varepsilon_{ii} + \varepsilon_{jj}).$$

The derivation of this equation is given in Ref. 14. We selected the exchange energies such that the surfactant head groups attract water and tail groups attract oil, analogous to the experimental situation. The silica species are designed to be more attractive towards the heads compared to water. In reality, the silica-head attraction depends on the system  $pH$ , which changes as silica polymerizes around the templates. Siperstein and Gubbins studied the influence of different silica interactions on the surfactant-water-silica phase diagram. In our work, we are interested in the equilibrium properties of the surfactant-water-silica system, which do not depend on the dynamical changes the system undergoes in reaching the final state. We have therefore assumed the silica interaction to be constant throughout the simulations. The first part of Table I gives the exchange energies, which are determined based on the criteria previously discussed. On the basis of the exchange energies, we then calculate the interaction potentials given in the second part of Table I.

The dimensionless temperature is defined as  $T^* = k_B T / w_{HT}$ , where  $w_{HT}$  is the coarse-grained interaction potential between a head and a tail beads. We selected  $T^* = 7.0$ , which provides an appropriate balance between the tail-tail attraction and entropic forces leading to the formation of the liquid-crystal phases.

We carried out lattice Monte Carlo simulations in a  $NVT$  ensemble, following the pathway of Larson *et al.* Three different types of moves were employed, which include the reptation, twist, and chain regrowth by configurational bias.<sup>17</sup> Similar to Kim *et al.*, we find the configurationally biased

TABLE I. Intermolecular interactions used in the lattice Monte Carlo simulations. (a) Exchange energies and (b) Interaction potentials. *H*: head, *T*: tail, *O*: oil, *W*: water, and *S*: silica.

(a)	$w_{ij}$	<i>H</i>	<i>T</i>	<i>O</i>	<i>W</i>	<i>S</i>
	<i>H</i>	0	1	1	0	-2
	<i>T</i>	1	0	0	1	1
	<i>O</i>	1	0	0	1	1
	<i>W</i>	0	1	1	0	0
	<i>S</i>	-2	1	1	0	0
(b)	$\epsilon_{ij}$	<i>H</i>	<i>T</i>	<i>O</i>	<i>W</i>	<i>S</i>
	<i>H</i>	0	0	0	0	-2
	<i>T</i>	0	-2	-2	0	0
	<i>O</i>	0	-2	-2	0	0
	<i>W</i>	0	0	0	0	0
	<i>S</i>	-2	0	0	0	0

moves essential for fast equilibration of the system. Most of these simulations were carried out in elongated boxes with one side much longer (eight times) than the other two sides. This minimizes the formation of curved interfaces, facilitating the measurement of phase properties like component concentrations. The box sizes and simulation times depend on the length scales of the structures produced. We have carefully chosen the simulation box dimensions so that we see at least three unit cells in the final configuration. Some of the simulations were carried out in larger boxes to verify that the configurations are independent of the box sizes. For a given surfactant concentration, we carried out the simulations using two different box sizes, where the larger box was two times the length of the smaller box. In both cases, we found the same equilibrium structure with similar pore sizes irrespective of the box lengths. Cylindrical and lamellar structures required a box size of  $30 \times 30 \times 240$ , whereas the mesocellular structures required larger boxes, typically  $60 \times 60 \times 480$ , because these structures are two to three times larger than the cylindrical structures. The equilibration times varied also, depending on the structures and box sizes used. Smaller boxes and cylindrical structures needed  $10^{10}$  Monte Carlo moves to equilibrate. For larger boxes and mesocellular structures, this number was about  $5 \times 10^{10}$  moves.

Once the system was equilibrated, we calculated the component concentrations, micellar size distribution, and the pore size distribution. Phase compositions were calculated by developing concentration profiles along the longest edge of the simulation box. The phase concentrations were then obtained by averaging over the local concentrations away from the phase boundaries. Micellar size distribution was measured using the cluster labeling algorithm by Hoshen and Kopelman.<sup>18</sup> The pore size distribution was obtained by rolling spheres of variable sizes along the surface of the pores. The cumulative pore size distribution is obtained by plotting the diameter of the largest sphere that can be fitted at a certain point inside the pore<sup>19,20</sup> against the cumulative pore volume. We then calculated the pore size distribution from the slope of the cumulative pore size distribution.

### III. RESULTS AND DISCUSSION

We first present the results for the simplest system, followed by the more complex ones. We start by describing the thermodynamic behavior of the surfactant  $H_3T_5H_3$  dissolved in water. Then, we add oil to the system and discuss the ternary phase diagram. Finally, we study the quaternary system, comprising surfactant, oil, water, and silica, where we see the appearance of the MCF structures. We conclude by analyzing the properties of the model MCF structure and comparing them with those of the experimental material.

#### A. Surfactant-water mixtures

The surfactant-water phase diagrams are obtained from *NVT* simulations carried out at different concentrations and temperatures. Figure 2(a) represents the aqueous phase diagram of the surfactant  $H_3T_5H_3$ , whereas Fig. 2(b) represents the phase diagram for  $H_2T_7H_2$ , having a different architecture. Figure 2(b) will be discussed in Sec. III B, where we compare the two phase diagrams. In Fig. 2(a), we see the concentration and temperature dependences of the various self-assembled structures starting from spherical micelles at low concentrations and evolving into cylindrical and lamellar structures at higher concentrations. As the temperature is increased, there is a transition from ordered self-assembled structures to a completely homogeneous phase. The approximate zone of this transition is between  $T^* = 7.0$  and  $8.0$ , which is marked by the solid curves with an error bar on  $T^*$  equal to  $0.5$ . The features are similar to those found in the experimental phase diagrams for nonionic surfactants as well as the simulation results for diblock surfactants.<sup>15,13</sup>

Micellization is observed at low surfactant concentrations. We can distinguish between the spherical and the elongated micelles by viewing the simulation box snapshots. Initially these micelles are spherical, but they become elongated at higher concentrations. Around 60% surfactant concentration, they transform into hexagonally ordered infinite cylinders. Figure 3 shows the aggregation number distributions at different concentrations. At 5% concentration, the micelles are just starting to appear, as indicated by the plateau in the distribution curve. At 20%, the curve shows a sharp peak with the median around 25 chains. At the same time, there is an extended plateau at higher cluster sizes indicating the presence of elongated micelles. At 40% surfactant concentration, the distribution becomes wider and the plateau becomes more prominent as the micelles become increasingly ellipsoidal.

We observe the existence of hexagonally ordered cylindrical structures between 60% and 80% concentrations. Above 80%, the lamellar structures are observed. Between 80% and 90% concentrations, there is likely to be a transition region where cubic structures exist. However, observing such structures requires a careful selection of the box dimensions and longer simulation times.

#### B. Effect of head and tail lengths

In order to study the effect of surfactant architecture on self-assembly, we studied the aqueous phase diagrams of two different triblock surfactants with the same overall length but

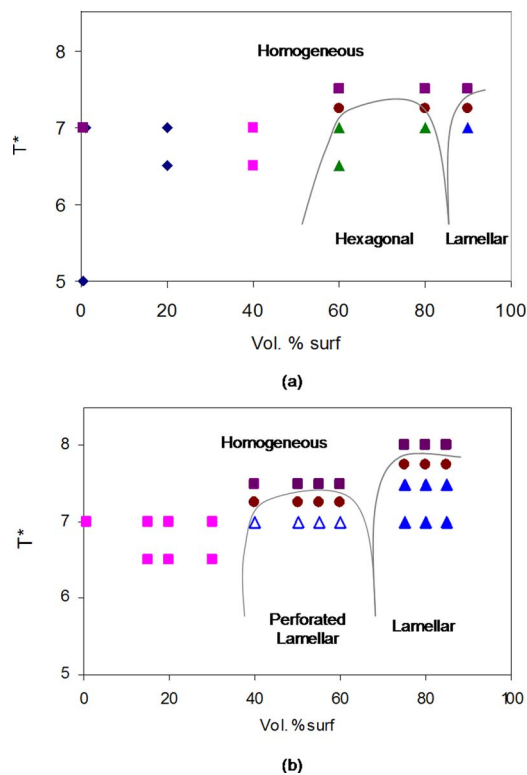


FIG. 2. (Color online) Surfactant-water binary phase diagrams. (a)  $H_3T_5H_3$  and (b)  $H_2T_7H_2$ . The symbols are used to represent the various ordered phases. Phase boundaries are marked using grey lines: ( $\blacklozenge$ ) Spherical micelles, ( $\blacksquare$ ) elongated micelles, ( $\blacktriangle$ ) hexagonal phase, ( $\blacktriangleleft$ ) perforated lamellae, ( $\blacktriangleright$ ) lamellar phase, ( $\blacksquare$ ) disordered, and ( $\bullet$ ) phase boundary.

different head and tail lengths (Fig. 2). One was  $H_2T_7H_2$ , which has seven tail units with two head units on both sides and  $H_3T_5H_3$  which has five tail units with three head units on either side. At low surfactant concentrations, both  $H_2T_7H_2$  and  $H_3T_5H_3$  form spherical micelles, which become ellipsoidal with the increase in surfactant concentration. Both surfactants create ordered self-assembled structures at higher concentrations. While  $H_2T_7H_2$  forms only lamellar structures,  $H_3T_5H_3$  forms both cylindrical and lamellar structures. In the  $H_2T_7H_2$ -water phase diagram, the perforated lamellae are observed at medium surfactant concentrations, whereas regular lamellae are observed at high surfactant concentrations. A comparison between the structures formed by the two surfactants indicates that  $H_2T_7H_2$  has more affinity towards the lamellar structures compared to  $H_3T_5H_3$ . This is in direct agreement with the experimental data published by Wanka and Ulbricht,<sup>21</sup> which suggests that surfactants with longer head groups favor the formation of curved interfaces, e.g., cylinders, whereas surfactants with small head groups favor the structures having flat interfaces, e.g., lamellae.

### C. Surfactant-oil-water mixtures

The ternary phase diagram for the  $H_3T_5H_3$ -oil-water system is shown in Fig. 4(a). Spherical micelles are observed at low oil and surfactant concentrations. Elongated micelles and hexagonal arrangements of cylindrical micelles are observed at medium surfactant concentrations near the surfactant-water side of the phase diagram. Starting from the

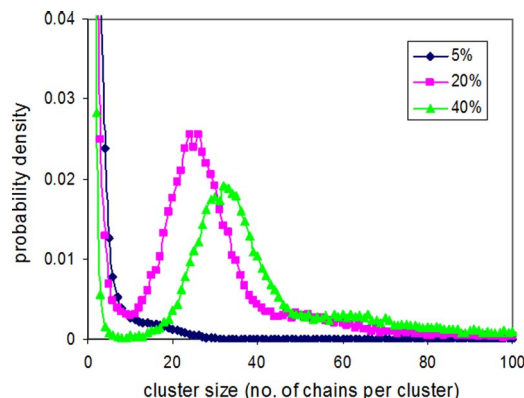


FIG. 3. (Color online) Aggregate size distributions at different surfactant concentrations.

hexagonal phase on the surfactant-water side, as we move towards high oil concentrations, we find the emergence of a lamellar phase. In our simulations, bicontinuous structures appeared only in one point on the phase diagram, although we believe that extensive simulations should be able to find additional points. It must be noted that, the transitions between the different self-assembled structures cannot be called the true thermodynamic phase transitions because they are not the first order in nature. Phase separation is observed on the surfactant-oil side between a dilute surfactant solution and a surfactant-rich phase. The characteristics of the phase diagram are highly dependent on the interactions of the oil with the other components in the system.

### D. Surfactant-water-silica and oil mixtures

Silica is added to the system as a fourth component. In our simulations, silica is more attractive towards the surfactant headgroups than water ( $\epsilon_{HS}=-2$  and  $\epsilon_{HW}=0$ ). The surfactant-water-silica phase diagram is shown in Fig. 4(b). Due to the higher head-silica attraction as compared to the head-water attraction, we observe the phase separation between a surfactant-rich silica-rich phase, and a water-rich phase. Ordered phases that are observed at different regions of the phase diagram depend on the component concentrations. Spherical micelles are found at low to medium surfactant concentrations, bicontinuous structures are observed at high surfactant, high silica concentrations, whereas cylindrical structures are seen at high surfactant, high water concentrations. When the number of system components increases to four, it is no longer possible to represent the phase diagram in two dimensions. A tetrahedron needs to be constructed with each corner representing one component. In this phase diagram, we limit ourselves to the region which is favorable for the formation of the mesocellular structures. We mimicked the experimental pathway by starting from zero oil concentration on the surfactant-water-silica phase diagram. We selected this initial point in the region of the hexagonal phase because experimentalists have reported the silica structure to be hexagonal in the absence of oil. The oil concentration is now increased in small increments, keeping

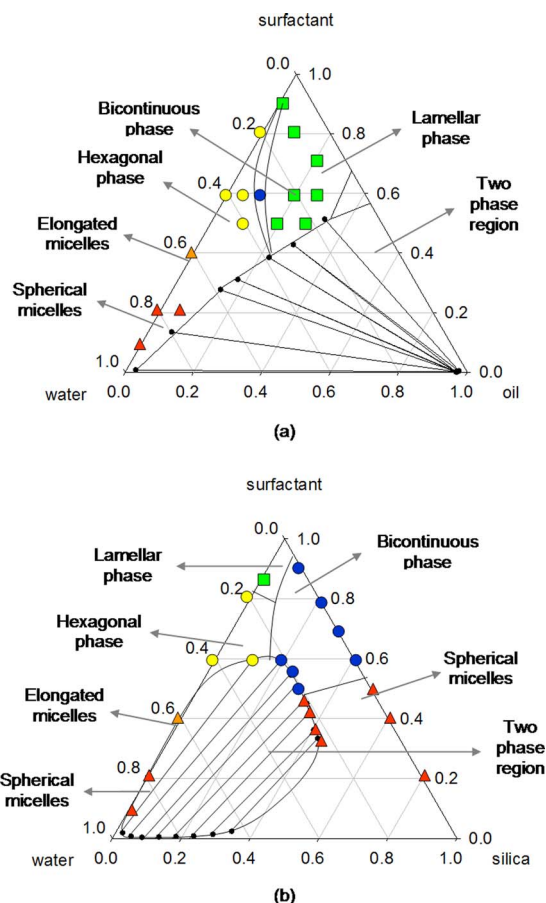


FIG. 4. (Color online) (a) Surfactant-oil-water phase diagram and (b) surfactant-silica-water phase diagram, the simulation points are shown as follows: ( $\blacktriangle$ ) spherical micelles, ( $\triangle$ ) elongated micelles, ( $\circ$ ) cylindrical micelles, ( $\bullet$ ) bicontinuous phase, and ( $\square$ ) lamellar phase. The phase boundary lines are provided as a guide to the eyes.

the proportion of the other components constant. The structures which we observe are depicted in Fig. 5 along with the experimental findings.

Figure 5(1) shows the simulation box snapshots at different oil concentrations. Below 10% concentration, the structures are cylindrical, whereas between 10% and 16%, they are lamellar. Both the cylindrical and lamellar structures have pore sizes of the same order of magnitude. Around 16% oil concentration by volume, the structure becomes mesocellular. Figure 5(1)(a) is the view of a cross section of the simulation box showing the pore walls of the model MCF. For better visualization, the box has been extended to include two adjacent periodic images. All three snapshots are of the same scale. The mesocellular pores are 2.5 times larger compared to the cylinders and the lamellae. Figure 5(2) shows the experimental results from Lettow *et al.* In both the simulations and the experiments, the cylindrical structures are observed at low oil levels and these structures transform into mesocellular foams once the oil concentration is increased. However, the transition from cylinders to mesocells follows separate pathways in the simulations and the experiments. According to the experimental results reported by Lettow and co-workers, undulations occur in the walls of the cylinders prior to the transformation to MCF similar to Fig. 5(2)(b). These undulations appear at medium oil concentra-

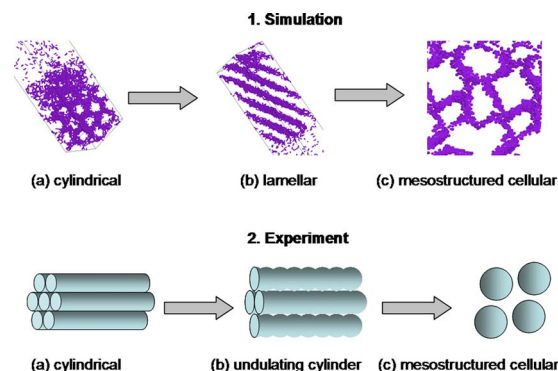


FIG. 5. (Color online) (1) Simulation: Change in pore structure with increasing oil concentration. (a) 2%, (b) 9%, and (c) 23%. (2) Experiment: Change in pore structure with increasing oil/surfactant mass ratios as reported in Ref. 6. (a) 0.00, (b) 0.21, and (c) 0.50.

tions, becoming more prominent as the oil concentration is increased. Finally the cylinders get pinched off at regular intervals producing isolated spheres. In the simulations, we did not observe the undulating cylinders at medium oil concentrations, but found a lamellar phase in that region. While it is difficult to explain the transition observed in the experiments, the simulation system shows predictable behavior. The geometrical shapes adopted by surfactant phases depend on the head-tail interfacial curvature and is discussed in details by Israelachvili.<sup>22</sup> The cylinders are formed at low oil concentrations, where the surfactant tails prefer to stay together, whereas the heads are solvated by water molecules. This leads to a very strong head-tail interfacial curvature leading to the formation of the cylinders. As oil is introduced into the system, the tails become solvated by the oil molecules, which increases the volume of the hydrophobic part of the micelles. This decreases the head-tail curvature favoring the formation of geometric shapes with low interfacial curvatures, such as the lamellae. The transition from the lamellae to the mesocells is, however, more complicated and requires further investigation. The exact mechanism for the formation of the mesocellular structures is not fully clear. Till now, what we have understood may be summarized as follows. As the amount of oil is increased in the system, due to the reasons explained in the later sections, the surfactant-rich phase is forced to maintain high oil concentrations. The mesocells are a result of the surfactant chains trying to shield the hydrophilic heads from being in contact with the oil molecules at such high oil concentrations. At low oil concentrations, the surfactants can orient themselves in cylindrical or lamellar structures and thus protect the heads from coming into contact with oil. In those structures, the hydrophobic parts of the micelles remain solvated by the oil molecules. However, at high oil concentrations, the amount of oil in the system exceeds the capacity of the tails to dissolve oil. Therefore, the surfactants form structures with pure oil cores surrounded by coronas of oil saturated tails, similar to the mesocells.

In order to understand the formation of the self-assembled structures in the presence of oil, we need to examine the compositions of each phase in the two phase separated quaternary system. Table II lists the phase compositions

TABLE II. Compositions of different components in the quaternary surfactant-oil-water-silica system. The letters denote the structures observed in the surfactant-rich phase. *C*: cylindrical, *L*: lamellar, and *M*: mesocellular.

Initial composition (vol %)				Phase 1 (vol %)				Phase 2 (vol %)			
Surfactant	Oil	Water	Silica	Surfactant structure	Oil	Water	Silica	Surfactant	Oil	Water	Silica
20.0	0.0	75.0	5.0	61.0- <i>C</i>	0.0	28.0	11.0	1.5	0.0	96.5	2.0
19.6	1.96	73.53	4.9	56.0- <i>C</i>	3.5	30.0	10.5	0.6	1.0	96.0	2.3
18.18	9.09	68.18	4.55	51.0- <i>L</i>	22.0	18.0	9.0	0.5	3.0	94.0	2.5
17.39	13.04	65.22	4.35	43.0- <i>L</i>	28.0	20.0	9.0	0.5	2.8	94.2	2.5
16.67	16.67	62.5	4.17	40.0- <i>M</i>	33.0	20.0	7.0	0.5	3.0	94.3	2.2
15.38	23.08	57.69	3.85	34.0- <i>M</i>	43.0	17.0	6.0	0.6	3.2	94.0	2.2

along with the starting concentrations. Phase 1 denotes the surfactant-oil-rich phase and phase 2 denotes the water-rich phase. When both silica and oil are present in the system, we observe the phase separation between a surfactant-rich phase and a water-rich phase. However, in the absence of silica, phase separation leads to an oil-rich phase instead of the water-rich phase. If we compare the above two situations, we notice the difference in behavior that is brought about by the introduction of silica into the system. In the surfactant-oil-water system, the surfactant is clearly water soluble, but when silica is added, the surfactant phase becomes oil soluble. Even a very small amount of silica (less than 5% by volume) is able to increase the oil solubility of the surfactant to significant levels. Interestingly, the mesocellular structures are a result of the high oil concentration in the surfactant-rich phase. An important question arises here. Why is the mesocellular phase not observed in the surfactant-oil-water system? The answer is that, in the absence of silica, the surfactant phase is unable to maintain the high oil concentrations necessary for the formation of the mesocells. In the surfactant-oil-water phase diagram, increasing the amount of oil leads to a transition from the hexagonal phase to the lamellar phase. Any further increase in oil concentration leads to a phase separation and the additional oil goes to the dilute phase. Now, consider the four component system. Silica helps to maintain high oil levels in the surfactant phase. At a very high oil concentration, the lamellar phase becomes unstable because the amount of oil exceeds the saturation point of the tails. At this stage, the system is expected to form reverse micelles in oil with heads inwards and tails outwards. However, in this arrangement, the head segments of surfactants in adjacent micelles are free to overlap, thus decreasing the transnational entropy of the system. As a result, the reverse micellar configuration is energetically less favorable compared to the mesocellular phase. This also suggests that it may not be possible to synthesize MCFs using diblock surfactants. For the diblock surfactants, the entropic constrain for the reverse micellar phase does not exist. Therefore, at high oil concentrations, the diblock surfactants are able to form reverse micelles instead of the mesocellular phase.

## E. Pore size distributions

In order to determine how realistic our model is, we compare the pore size distributions (PSDs) of the model structures with those of the real materials. In Fig. 6(1), we

present the PSDs of two different structures: (a) the cylindrical structure produced at an oil concentration of 2% by volume, and (b) mesocellular structures produced at an oil concentration of 23% by volume. The cylindrical structures have a pore diameter of about 200 Å, while the mesocells have a pore diameter of 700 Å. Figure 6(1)(b) shows the PSD for the MCF. Due to the presence of the smaller windows and the relatively larger cell cavities, we find two distinct peaks in the pore size distribution. The one at 300 Å corresponds to the window diameter, whereas the one at 700 Å represents the cell diameter. Figure 6(2) is the pore size distribution of an experimental MCF structure obtained from literature. The experimental structure also shows two peaks, one at 194 Å and the other at 410 Å. On analyzing the PSDs of the model silica structures, we find qualitative agreement with the experimental results. Both the model and the real MCF structures show bimodal pore size distributions with sharp peaks. In the model PSD, the peaks are wider than those from the experiment. Also, besides the two larger peaks, the model PSDs show small peaks all over the distribution. These peaks arise because, in a lattice model, the silica particles are allowed to occupy only discrete positions in space.

In Fig. 7 we show how the average pore size changes with oil concentration, both in the simulations and in the

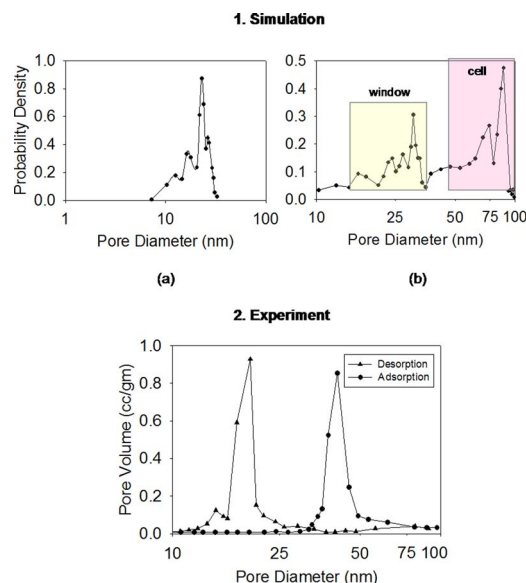


FIG. 6. (Color online) (1) Simulation: Pore size distributions of two different structures. (a) Cylindrical and (b) mesocellular. (2) Experiment: Pore size distribution of MCF material obtained by nitrogen adsorption.

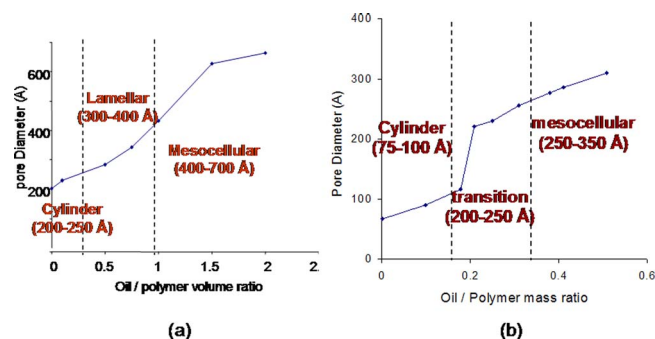


FIG. 7. (Color online) Average pore size with oil/surfactant ratio. (a) Simulation and (b) experiment.

experiment. In both situations, the pore size increases monotonically as the oil concentration is increased. Figure 7(a) represents the simulation results. At low oil/polymer ratios, we observe the cylindrical pores with diameters 200–250 Å. The pore size increases to 300 Å as we move to the lamellar region. Finally, in the mesocellular region, we find very large pores with diameters around 400–700 Å. Comparing with the experimental results [Fig. 7(b)], cylindrical pores have diameters between 75 and 100 Å. In the transition region, the pores have a diameter around 250 Å, whereas the MCF structures have diameters between 250 and 350 Å. We find the pore sizes in the simulations to be over predicted compared to the experiments. This can be due to the inaccuracies in mapping the lattice parameters with the experimental dimensions. However, the relative increase in pore diameter from cylinders to mesocells is the same in both simulation and experiment. In simulation, the average mesocell diameter is 650 Å, which is 2.6 times that of the cylinders (250 Å). In experiment, the average mesocell diameter is 300 Å, which is three times that of the cylinders (100 Å).

#### IV. CONCLUSION

We have developed a molecular model for the synthesis of mesoporous silicas and specifically for the mesostructured cellular foams. Our model is based on the fundamental aspects of statistical thermodynamics, and is free from any prior assumption. Using lattice Monte Carlo simulations, we are able to elucidate the basic features of the surfactant-oil-water-silica systems without the need of rigorous atomistic simulations. We find that adding a strongly hydrophilic substance such as silica to the surfactant-oil-water system can significantly enhance the oil solubility of the surfactant. The MCF model obtained through lattice simulations shows a qualitative agreement with the experimental results, and reproduces the following aspects: (1) pore diameter increases

with increasing oil concentration, and (2) the statistical distribution of the pore sizes. Correct statistical pore size distributions are difficult to obtain using geometric mean-field models, which are at the same time essential for obtaining characteristics such as adsorption and other physicochemical characteristics of the pore system. In future, we plan to explore the entire quaternary phase diagram to locate the exact region of formation of the various silica structures, and to throw more light on the synthesis mechanism of the MCF materials.

#### ACKNOWLEDGMENTS

We would like to express our gratitude towards Henry Bock, Flor Siperstein, Lauriane Scanu, and Naresh Chenamsetty for many helpful discussions. This work was funded by Department of Energy (DOE) under Grant No. DE-FG02-98ER14847. Supercomputing time was provided by the National Partnership for Advanced Computational Infrastructure (NPACI) under Grant No. MCA93S011.

- <sup>1</sup>V. Chiola, J. E. Ritsko, and C. D. Vanderpool, U.S. Patent 3,556,725 (January 1971).
- <sup>2</sup>T. Yanagisawa, T. Shimizu, K. Kuroda, and C. Kato, *Bull. Chem. Soc. Jpn.* **62**, 1535 (1990).
- <sup>3</sup>C. T. Kresge, M. E. Leonowicz, W. J. Roth, J. C. Vartuli, and J. S. Beck, *Nature (London)* **359**, 710 (1992).
- <sup>4</sup>J. S. Beck, J. C. Vartuli, W. J. Roth *et al.*, *J. Am. Chem. Soc.* **114**, 10834 (1992).
- <sup>5</sup>Q. Huo, D. I. Margolese, and G. D. Stucky, *Chem. Mater.* **8**, 1147 (1996).
- <sup>6</sup>J. S. Lettow, Y. J. Han, P. Schmidt-Winkel, P. Yang, D. Zhao, G. D. Stucky, and J. Y. Ying, *Langmuir* **16**, 8291 (2000).
- <sup>7</sup>P. Schmidt-Winkel, W. W. Lukens, Jr., P. Yang, D. I. Margolese, J. S. Lettow, J. Y. Ying, and G. D. Stucky, *Chem. Mater.* **12**, 686 (2000).
- <sup>8</sup>P. Schmidt-Winkel, W. W. Lukens, Jr., D. Zhao, P. Yang, B. F. Chmelka, and G. D. Stucky, *J. Am. Chem. Soc.* **121**, 254 (1999).
- <sup>9</sup>S. Bhattacharya and K. E. Gubbins, *Stud. Surf. Sci. Catal.* (to be published).
- <sup>10</sup>D. Zhao, Q. Huo, J. Feng, B. F. Chmelka, and G. D. Stucky, *J. Am. Chem. Soc.* **120**, 6024 (1998).
- <sup>11</sup>A. Z. Panagiotopoulos, M. A. Floriano, and S. K. Kumar, *Langmuir* **18**, 2940 (2002).
- <sup>12</sup>S. Y. Kim, A. Z. Panagiotopoulos, and M. A. Floriano, *Mol. Phys.* **100**, 14 (2002).
- <sup>13</sup>F. R. Siperstein and K. E. Gubbins, *Mol. Simul.* **27**, 339 (2001).
- <sup>14</sup>F. R. Siperstein and K. E. Gubbins, *Langmuir* **19**, 2049 (2003).
- <sup>15</sup>R. G. Larson, L. E. Scriven, and H. T. Davis, *J. Chem. Phys.* **83**, 2411 (1985).
- <sup>16</sup>R. G. Larson, *J. Phys. II* **6**, 1441 (1996).
- <sup>17</sup>D. Frenkel and B. Smit, *Understanding Molecular Simulation*, 2nd ed. (Academic, New York, 2002).
- <sup>18</sup>J. Hoshen and R. Kopelman, *Phys. Rev. B* **14**, 3438 (1976).
- <sup>19</sup>L. D. Gelb and K. E. Gubbins, *Langmuir* **14**, 2097 (1998).
- <sup>20</sup>L. D. Gelb and K. E. Gubbins, *Langmuir* **15**, 305 (1999).
- <sup>21</sup>G. Wanka and W. Ulbricht, *Macromolecules* **27**, 4145 (1994).
- <sup>22</sup>J. Israelachvili, *Intermolecular and Surface Forces*, 2nd ed. (Academic, London, 1991).